

Geostatistics on Unstructured Grids: Application to Teapot Dome

John G. Manchuk

This work demonstrates some of the developments made in using geostatistical techniques to populate unstructured grids with reservoir properties. Data made available by the Rocky Mountain Oilfield Testing Centre (RMOTC) and U.S. Department of Energy is used for this study. It is from the federally owned Naval Petroleum Reserve No. 3, also called the Teapot Dome field. The Tensleep formation is the focus of this application. The study progresses through many of the typical steps involved in geostatistical modeling with unstructured grids.

1. Introduction

The purpose of this application is to demonstrate the use of geostatistics to populate unstructured grids with reservoir properties. Many of the steps involved are common to any geostatistical reservoir modeling workflow. They include data assembly, structural modeling, space transformation, upscaling from data scale to modeling scale, and statistical analysis. Upscaling from data scale to modeling scale is different because a regular or structured grid is no longer involved. Properties are upscaled to a common scale rather than to grid elements. New steps involved include grid refinement to handle the variety of scales introduced by unstructured grids, property modeling using geostatistics on irregular point sets, and upscaling from the refined grid to the unstructured grid for variables that average arithmetically. Refinement is done with a tetrahedral grid and geostatistical modeling algorithms are adapted to populate it. The centers of the tetrahedral elements form the irregular point set that is modeled.

The data for this study was provided by the Rocky Mountain Oilfield Testing Centre (RMOTC) and U.S. Department of Energy. It has been used in other research and studies as well (Olsen et al, 1993; Garcia, 2005; Friedmann and Stamp, 2006). The field is referred to as the Teapot Dome field and it consists of several geological units. The Tensleep formation is the focus of this application.

Three types of data are available: core, geophysical logs, and 3D seismic. Variables derived from the core that are used include horizontal permeability k_h , vertical permeability k_v , porosity ϕ , water saturation S_w , and oil saturation S_o . Of the available logs, those used include gamma ray (GR), bulk density (RHOB), neutron porosity (NPHI), deep resistivity (RD), and shallow resistivity (RS). There are 37 wells that intersect the Tensleep formation, 31 of them with logs and 18 with core. The boundary of the Tensleep Dome formation, topography, and wells are shown in Figure 1. Seismic covers the whole area and is used for structural modeling. Horizons for the Tensleep top and base are available in the time domain. Available well markers are used to convert the horizons from time to depth.

Log scale data is used for modeling. The logs are processed into four reservoir properties including lithology, porosity, water saturation, and oil saturation. Continuous properties are modeled using geostatistical methods. Lithology consists of sand and dolomite and is assigned based on well markers. There are four markers, ASand, BDolo, BSand, and C1Dolo ordered by increasing depth. Other logs are processed using standard procedures and calibrated using the core data (Ellis and Singer, 2007).

2. Structural Modeling

Horizons of the Tensleep top and base, respectively the ASand and C1Dolo markers, interpreted from the seismic data are available in the RMOTC data set in the time domain. These horizons were converted to the depth domain using the well markers. Based on the seismic, there are also several faults in the formation; however, the data set did not include any fault interpretations. Six faults were interpreted from the seismic by hand. Contour maps of the top and base structure are shown in Figure 2. The structure is an anticline that trends North North-West. Faults in the modeling area identified in Figure 2 have the largest vertical offset, up to 100 feet near mile 151.8 in East and 180.5 in North.

Horizons and faults are used to map from physical space to depositional space. Stratigraphic coordinates are used, but to account for the faulting and deformation of the horizons, they are applied with a background tetrahedral grid. The stratigraphic coordinate system axes are labelled u, v, t . Within the modeling area, the following surfaces were triangulated: top, base, two faults, and model boundary. These surface are stitched together to form a sealed model that is used to produce the background tetrahedral grid (Figure 3). Nodes of the

tetrahedral grid are assigned depositional coordinates. All nodes on the top receive a value of zero while all those on the base receive a depth of 110 feet, which is approximately the average thickness of the formation. Stratigraphic coordinates of any interior tetrahedron nodes are assigned by interpolation. Mapping a point from physical space to depositional space involves the following steps:

1. Find the tetrahedron containing the point, \mathbf{u} .
2. Compute the barycentric coordinates of the point, $L = \{L_1, L_2, L_3, L_4\}$.
3. Interpolate the depositional coordinates from the tetrahedron nodes, $t = \{t_1, t_2, t_3, t_4\}$ to the point:
 $t_p = L^T t$.

Statistics used for reservoir modeling, including the property distribution and the variogram, are derived in depositional space. All well data is mapped to u, v, t space. Wells that are inside the modeling area are transformed using the tetrahedral grid method and standard stratigraphic coordinate mapping is applied to wells outside the area using Equation (1).

$$t = -\frac{z - z_{ASand}}{z_{ASand} - z_{C1Dolo}} \cdot 110 \quad (1)$$

3. Upscaling Logs to Modeling Scale

When unstructured grids are involved, it is suggested that well log data is upscaled into equal intervals along the well bore instead of into differently sized grid elements. The interval is chosen with two goals: to unify hard data to a single scale and avoid smoothing out important details. The highest level of detail possible is based on the log sample spacing that is sampled with 6 inch spacing along the well bores. Considering all wells, there are 6,579 samples at this resolution.

A variety of approaches can be used to determine a scale for geological modeling. One approach is to attempt to determine a representative element volume (REV) (Bear, 1972). Another possibility is to increase the scale until a specified amount of variability is removed from the data. In applications with regular grids, the scale may simply be chosen arbitrarily to limit the number of cells or it may be based on the resolution to be used in a flow simulator. In typical applications, regular grid cells are chosen between 10 and 50 meters horizontally and 0.1 to 1 meters vertically (Aarnes et al, 2007). In this study, the vertical resolution for upscaling the logs is chosen at 1.64 feet or 0.5 meters. Since the lithology is defined by well markers, no upscaling intervals are chosen to contain both indicators. Upscaling is done in the ASand-BDolo, BDolo-BSand, and BSand-C1Dolo intervals separately for each well.

4. Statistical Analysis

Processes applied to this data include declustering, data transformation (normal score transform), correlation analysis, and variogram modeling. A log ratio data transformation process is used for oil and water saturation since these variables form a composition.

Wells are clustered around the peak of the anticline structure and fairly sparse elsewhere. Cell declustering is applied in two dimensions since all wells are close to vertical and the formation thickness is relatively constant. Cell size choice is based on maximizing the mean of Vsh that is the only continuous property defined at all well locations. A declustering cell size and mean plot (Figure 4) indicates a maximum plateau is reached for a cell size of approximately 7,000 ft. This is in close agreement with the average well spacing of 7,124 ft. Using a cell size of 7,000 ft, the mean of Vsh is 0.243, an increase of 15% from the non-declustered mean.

The data are normal score transformed by lithology. Water saturation and oil saturation are not directly transformed to Gaussian space. In cases where the reservoir rock is fully saturated with two phases such as oil and water, it is only necessary to model one and the normal score transform can be used directly. In this case, there is water, oil and an additional phase since S_o and S_w do not sum to one. The unknown phase is labeled S_f and its value is $S_f = 1 - S_o - S_w$. These three phases form a composition and modeling the saturations as any other continuous variable provides no control on their sum. Several techniques exist to deal with compositional data (Pawlowsky-Glahn and Egozcue, 2006; Pawlowsky-Glahn and Olea, 2004). The additive logratio (ALR) transformation is used prior to the normal score transform to remove the sum constraint. Equation (2) defines the forward ALR transform and Equation (3) the inverse ALR transformation.

$$R_x = ALR(S_x) = \log\left(\frac{S_x}{S_f}\right), x = oil, water \quad (2)$$

$$S_x = ALR^{-1}(R_x) = \frac{\exp(R_x)}{\exp(R_w) + \exp(R_o) + 1}, x = oil, water \quad (3)$$

Prior to the ALR transform, saturations are properly visualized in a simplex or ternary diagram with its vertices defining each component at 100% saturation and the opposite sides defining 0% saturation. Post ALR transform S_w and S_o are plotted on Cartesian axes (Figure 5).

Correlation coefficients between ϕ , $ALR(S_w)$, and $ALR(S_o)$ are computed for each lithology using the normal scores (Table 1). Permeability models are constructed based on a regression equation between these properties rather than through Gaussian simulation because permeability at the log scale was not derived and permeability samples from core are sparse. Using linear regression, a quadratic relationship between ϕ and k_h is derived (Equation (4)) and a linear relationship between k_h and k_v (Equation (5)); Figure 6). Although this relationship was derived from core scale data, it is assumed to be valid for log scale data as well.

$$\log(k_h) = -164.07\phi^{3/2} + 135.79\phi - 7.23 \quad (4)$$

$$\log(k_v) = 0.79 \log(k_h) - 1.06 \quad (5)$$

Variogram modeling of the normal score variables results in the models defined in Table 2. For continuous variables, all models have a nugget effect of zero. All variograms are oriented with an azimuth of 160 degrees, corresponding to Range 1 in the table. Range 2 corresponds to an azimuth of 70 degrees and Range 3 is vertical.

Table 1: Correlations.

Lithology	ϕ -ALR(S_w)	ϕ -ALR(S_o)	ALR(S_w)-ALR(S_o)
Upper Sand	-0.524	-0.217	0.741
Dolomite	-0.505	-0.427	0.856
Lower Sand	-0.011	0.045	0.916

Table 2: Continuous property variogram models.

Lithology	Property	Structure	Variance	Range 1, ft	Range 2, ft	Range 3, ft
Upper Sand	ϕ	Exponential	0.2	500	1,000	5
		Spherical	0.8	5,000	2,500	40
	ALR(S_w)	Exponential	0.5	2,000	3,000	50
		Spherical	0.5	8,000	3,000	50
	ALR(S_o)	Exponential	0.4	2,000	3,000	50
		Spherical	0.6	8,000	3,000	50
Dolomite	ϕ	Exponential	0.6	3,000	1,500	20
		Spherical	0.4	5,000	3,000	400
	ALR(S_w)	Exponential	0.5	2,000	3,000	18
		Spherical	0.5	8,000	3,000	20
	ALR(S_o)	Exponential	0.4	2,000	3,000	25
		Spherical	0.6	8,000	3,000	30
Lower Sand	ϕ	Exponential	0.2	500	1,000	15
		Spherical	0.8	5,000	2,500	80
	ALR(S_w)	Exponential	0.5	2,000	3,000	18
		Spherical	0.5	8,000	3,000	80
	ALR(S_o)	Exponential	0.4	2,000	3,000	20
		Spherical	0.6	8,000	3,000	100

5. Unstructured Grid Design

Existing studies involving the Tensleep formation such as Friedmann and Stamp (2006) have evaluated it for enhanced recovery using CO₂ injection and CO₂ storage. The targeted area is in the shallowest portion of the anticline structure that acts as a trap for injected CO₂. For purposes of the demonstration, an arbitrary tetrahedral grid design is used. The grid has 24,247 points and 121,994 elements (Figure 7). Elements with smaller volume are concentrated in areas of expected high velocity and around the faults, assuming this type of information was available for flow based grid design.

Flow simulation could be applied to either the tetrahedral grid or the dual polygonal grid (Figure 8). Moreover, refinement results in the same high resolution grid for both coarse scale grids; therefore the geostatistical models would also be identical. The advantage of the tetrahedral grid is that the faults are honored by the element interfaces. Polygonal elements are bisected by the faults and incorporating information such as the flow character of the faults is difficult. On the other hand, the advantage of the polygonal grid is substantially fewer control volumes. Flow simulation would be done using 24,247 elements as opposed to 121,994. This case study carries on with the tetrahedral grid.

6. Grid Refinement

Refinement of individual cells is based on an error criteria derived from the variogram. The error measures the accuracy of the arithmetic average of the refinement within a coarse unstructured grid element. It is equivalent to the estimation variance that measures the error between true values and the estimate obtained by kriging. Achieving a user defined error criteria for all variables involved requires a variogram that is greater than all other variograms (Figure 9). The resulting error surface that relates tetrahedral element and number of refinement elements to error is shown in Figure 10 along with the selected contour that is used to control the refinement process.

A total of 1,241,152 points resulted from refinement, which is an average of 10 points per volume. No volumes received more than 20 points to keep the total number reasonable. In areas where smaller elements are located, the average tetrahedron volume is 4,389 ft³ and they are discretized by 4 points on average. Each point represents a volume of 1,097 ft³. To obtain such a resolution with a regular or structured grid would require a high resolution everywhere in the modeling domain. The whole reservoir has a volume of 10,495×10⁶ ft³, which would require a structured grid having upwards of 9.5 million elements. Based on the smallest tetrahedron volume, which is less than 10 ft³, a regular grid achieving this resolution would require more than one billion elements.

7. Property Modeling

For geostatistical modeling, barycenters of the refined grid elements are transformed to depositional space. Variables ϕ , ALR(S_w), and ALR(S_o) are modeled within each lithology. A program called `psgsim` was developed to do this using collocated cokriging for multiple continuous variables. Within each lithology, ϕ is modeled using simple kriging, followed by ALR(S_w) using collocated cokriging conditional to the simulated ϕ value, and finally ALR(S_o) conditional to ALR(S_w). Correlation coefficients shown in Table 1 were used. Twenty realizations were generated to show reproduction of distributions, bivariate relationships, and variograms. 18 data were used to construct systems of equations for kriging. Each realization took approximately 7.15 minutes on an Intel 2.13 GHz processor.

Distributions of each property are checked for shape and summary statistics including the mean and standard deviation. Reproduction of mean and standard deviation of continuous properties within each lithology is in Table 3. The fraction difference between true and simulated fluid saturations is high for Dolomite and upper sand. This is due to the ALR transformation process and is caused by the occurrence of zeros in the data. When S_w and S_o sum to 1, which occurred primarily when one of S_o and S_w was equal to 1, S_f is zero causing some stress with the ALR transform. Resulting distribution tails are visible in the distribution reproduction plots (Figure 11). Long tails on the saturation distributions account for a very small proportion of the realizations and only cause inflation in the variance; reproduction of the mean remains accurate. Otherwise, all realization distributions reproduce the input distributions well.

Variogram reproduction is not perfect in this application: some properties and directions match very well, while others have a mismatch (Figure 12). Only porosity variograms are shown and similar results were obtained for the other variables. Types of mismatch observed include: variograms having the correct shape, but not reaching the sill; variograms matching short range structure well, but depart from the input model with increasing

range; trouble with reproducing anisotropy; and variograms going over the sill, indicating variance inflation, which is a known issue with collocated cokriging. Causes of these are using a limited number of data for kriging, 18 in this case, possibly random path related, and attempting to enforce variogram reproduction for a multivariate study without using direct variograms from a linear model of coregionalization.

A final check is to ensure relationships between variables were preserved, which includes correlation coefficients and the shape of scatter plots. Unlike variograms and histograms, it is not feasible to create a scatterplot for all realizations so the tenth realization is shown. It is also difficult to see relationships when over 1.2 million points are plotted on a scatterplot. Instead, the realization results are converted to a density and plotted as contours. True data are plotted as points over the contours for a visual check (Figure 13). Contours appear to represent the density distribution from which the samples originated in all cases. Correlation coefficients are checked for all realizations (Table 4). Most coefficients are reproduced well, although the coefficient for $\phi-S_o$ in lower sand is low.

Table 3: Reproduction of mean and standard deviation.

Prop.	Lith	True Mean	Mean of Models	Fraction Diff	True σ	σ of Models	Fraction Diff
Phi	Upper S.	0.061	0.061	0.000	0.025	0.025	0.000
	Dolo	0.072	0.064	-0.111	0.040	0.035	-0.125
	Lower S.	0.106	0.105	-0.009	0.037	0.037	0.000
S_w	Upper S.	0.581	0.575	-0.010	0.088	0.106	0.205
	Dolo	0.505	0.515	0.020	0.106	0.144	0.358
	Lower S.	0.574	0.570	-0.007	0.078	0.072	-0.077
S_o	Upper S.	0.249	0.257	0.032	0.045	0.081	0.800
	Dolo	0.286	0.294	0.028	0.049	0.122	1.490
	Lower S.	0.262	0.264	0.008	0.033	0.029	-0.121

Table 4: Reproduction of correlation coefficients.

Pair	Lithology	True Correlation	Mean Simulated Correlation	Difference
Phi – S_w	Upper sand	-0.037	0.005	0.042
	Dolomite	-0.442	-0.537	-0.095
	Lower Sand	-0.591	-0.643	-0.052
Phi – S_o	Upper sand	0.089	-0.001	-0.090
	Dolomite	0.432	0.432	0.000
	Lower Sand	0.627	0.444	-0.183
S_o – S_w	Upper sand	-0.914	-0.946	-0.032
	Dolomite	-0.959	-0.928	0.031
	Lower Sand	-0.912	-0.857	0.055

8. Upscaling

An advantage of the proposed workflow is the simplicity of upscaling. There are no complex element intersections to be concerned with and covariance across all scales is preserved. Upscaling a structured grid to an unstructured grid requires many volume-volume intersection operations that are time consuming. In the case of flow based upscaling, velocities do not have to be interpolated to unstructured grid element interfaces because the fine scale velocities align exactly with the coarse element interfaces.

Realizations can be upscaled to either the tetrahedral grid or the dual polygonal grid. An advantage of upscaling to the polygonal grid is ease of visualization. Upscaled properties can be represented by the polygonal element centroids, which coincide with the tetrahedral grid vertices. Rendering models, generating cross sections, and performing other visualization operations are straightforward and computationally efficient in this case. Although resulting images are more visually appealing, the fact that properties are treated as constant within the control volumes must not be overlooked.

Lithology is upscaled to proportions, and ϕ , S_w and S_o are upscaled arithmetically. A realization of porosity is shown before and after upscaling (Figure 14). To move on with flow simulation, permeability would be computed from porosity and upscaled as well.

9. Conclusions

This case study demonstrated geostatistical modeling on unstructured grids. Instead of modeling reservoir properties on regular or structured grids, as in existing workflows, this approach uses a tetrahedral refinement of the unstructured grid design. Upscaling well data to the tetrahedral geological modeling grid is similar to existing workflows as data are upscaled to equal length volumes along the wells. This is identical to vertical wells through a regular grid. The difference is data are not upscaled to grid elements. A concern is scale discrepancy: the scale of upscaled well data is not equal to the scale of all tetrahedral elements in the refined grid. Simulated values represent the same scale as the upscaled data and estimates are made at the tetrahedral element centers. Considering the resulting values are used in upscaling, this is no different than discretizing a block into points for estimating an average covariance, or performing block kriging for example. Therefore, the scale discrepancy between upscaled well data and the refined grid is not a concern. A methodology to estimate the error of arithmetically averaging reservoir properties to the coarse unstructured grid elements was also shown. The measure is used to guide the grid refinement process.

Future work would be beneficial in several areas. The grid refinement process did not always complete successfully for several of the grid designs considered during the development of this application. Many refinement algorithms exist and should be tested; however, most are not geared towards geological modeling problems. Variogram reproduction was also not as good as expected. This requires further attention as the cause may be related to the random path, spatial search, associated input parameters, or a combination of these.

References

- Aarnes, J.E., Kippe, V., Lie, K.A., Rustad, A.B., 2007, Modelling of multiscale structures in flow simulations for petroleum reservoirs: Hasle G, Lie KA, Quak E (eds), Geometric Modelling, Numerical Simulation, and Optimization, Springer Berlin Heidelberg New York, pp. 307-360
- Bear, J., 1972, Dynamics of fluids in porous media: American Elsevier Publishing Company, 765 pp.
- Deutsch, C.V. and Journel, A.G., 1998, Geostatistical software library and user's guide. Oxford University Press, 384
- Ellis, D.V. and Singer, J.M., 2007, Well logging for earth scientists. Springer, 692 pp.
- Friedmann, S.J. and Stamp, V.M., 2006, Teapot Dome: characterization of a CO₂-enhanced oil recovery and storage site in Eastern Wyoming. The American Association of Petroleum Geologists, pp. 181-199
- Garcia, R.G., 2005, Reservoir simulation of CO₂ sequestration and enhanced oil recovery in the Tensleep formation, Teapot Dome field. Texas A&M University, 97 pp.
- Olsen, D.K., Sarathi, P.S., Hendricks, M.L., Schulte, R.K., Giangiaccomo, L.A., 1993, Case history of steam injection operations at Naval Petroleum Reserve No. 3, Teapot Dome Field, Wyoming: a shallow heterogeneous light-oil reservoir. Society of Petroleum Engineers, 25786, pp. 93-110
- Pawlowsky-Glahn, V. and Egozcue, J.J., 2006, Compositional data and their analysis: an introduction: Buccianti A, Mateu-Figueras G, Pawlowsky-Glahn V (eds), Compositional data analysis in the geosciences: from theory to practice: Geological Society, London, Special Publications, 264, pp. 1-10
- Pawlowsky-Glahn, V. and Olea, R.A., 2004, Geostatistical analysis of compositional data: Oxford University Press, 304 pp.

Figures

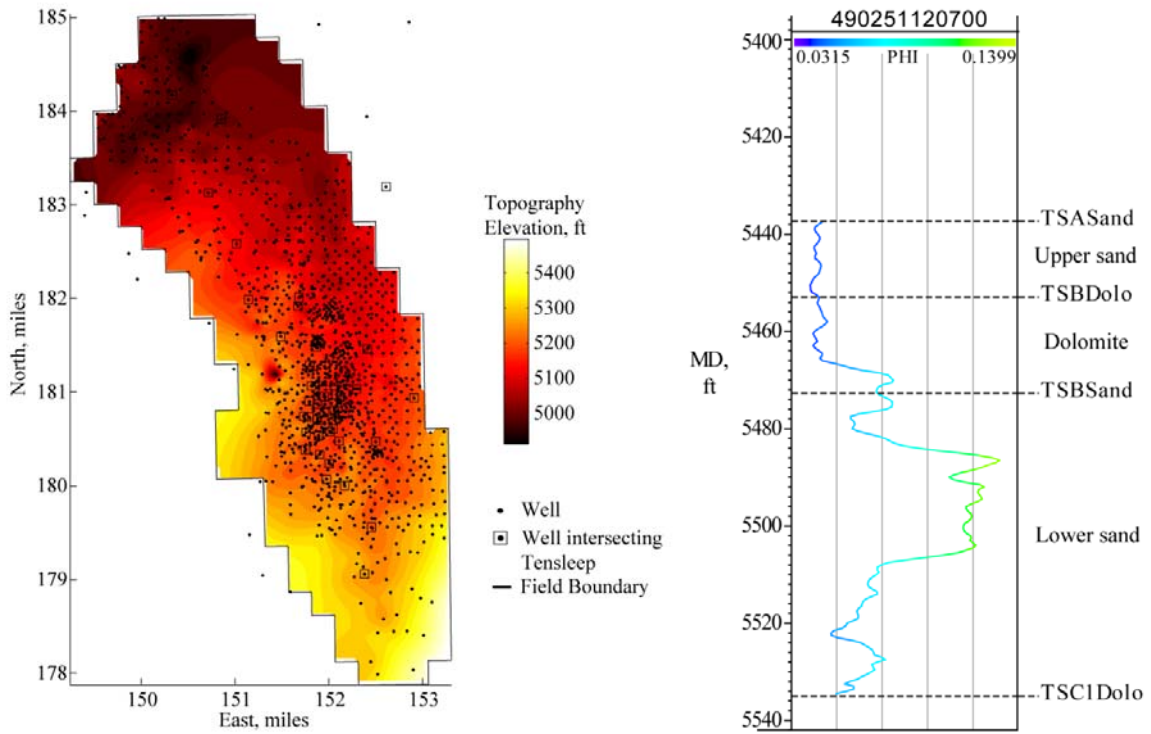


Figure 1: Teapot Dome field and well locations (left) and well tops (right).

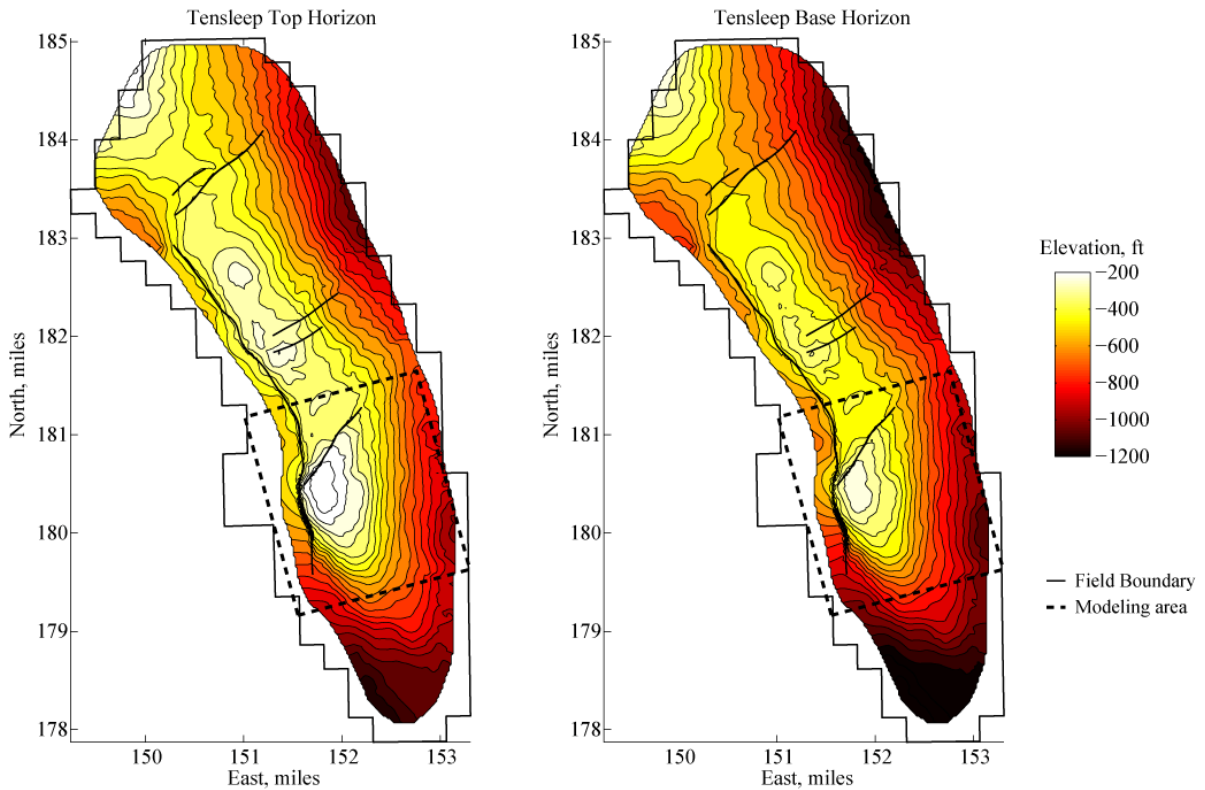


Figure 2: Tensleep horizons, fault traces, and modeling area.

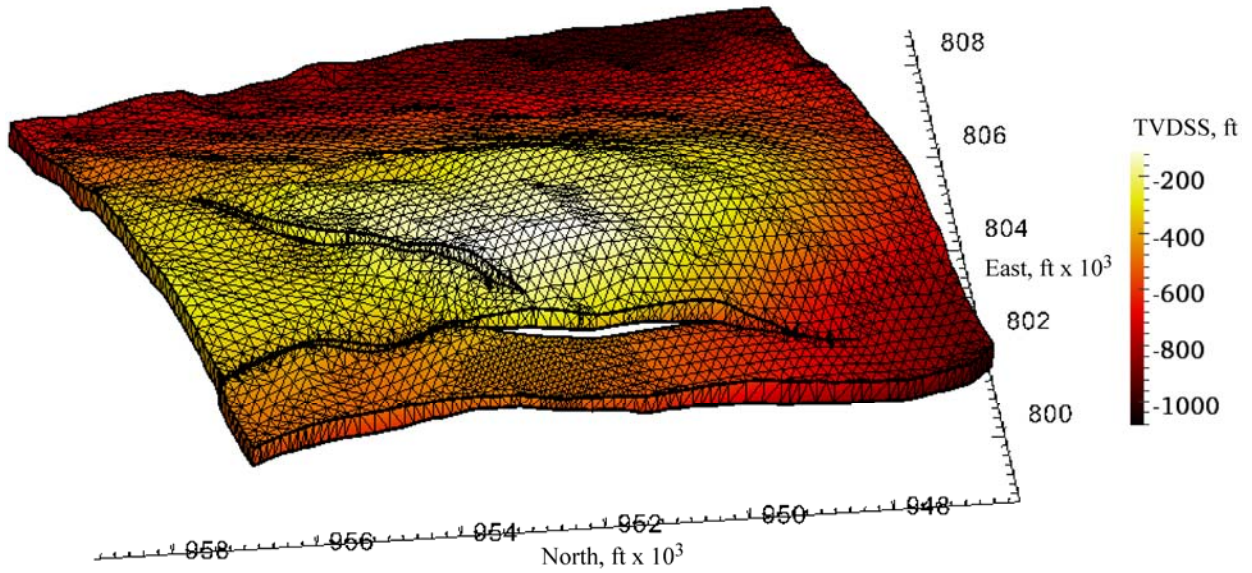


Figure 3: Isometric view of the tetrahedral grid generated for mapping from geological space to depositional space. A vertical exaggeration of three is used.

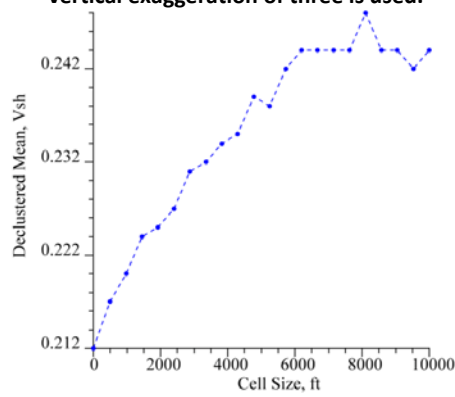


Figure 4: Declustering results.

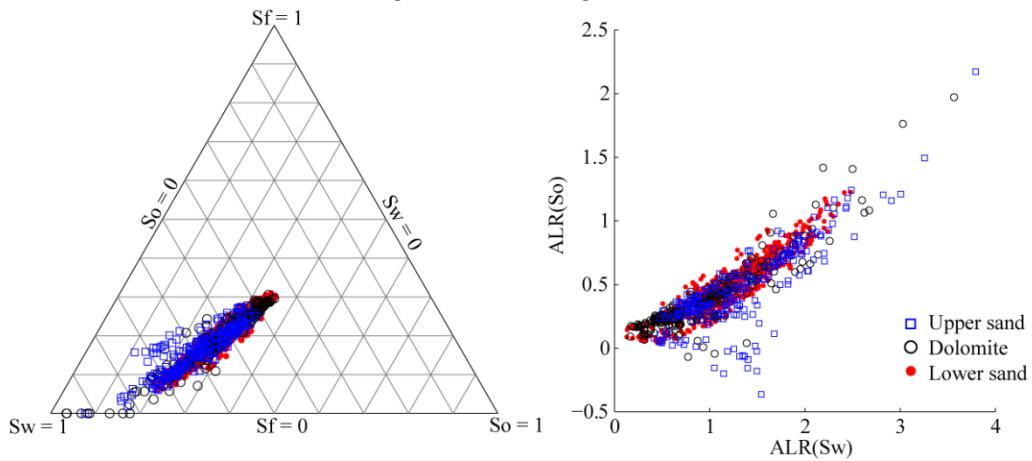


Figure 5: Ternary plot of saturations and ALR transformed cross plot.

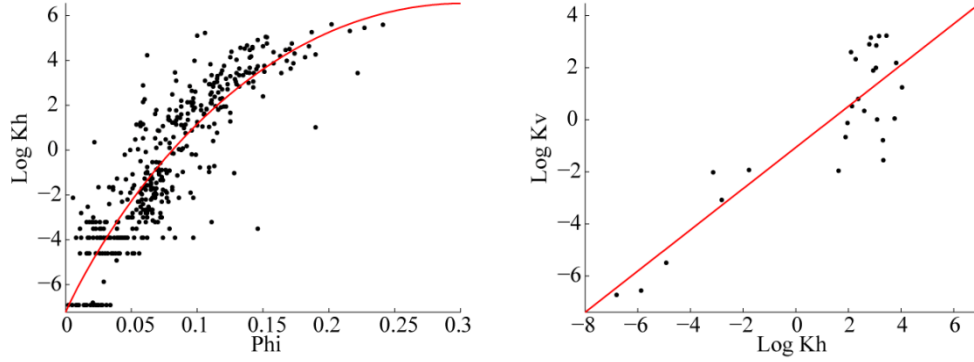


Figure 6: $\phi-k_h$ and k_h-k_v relationships.

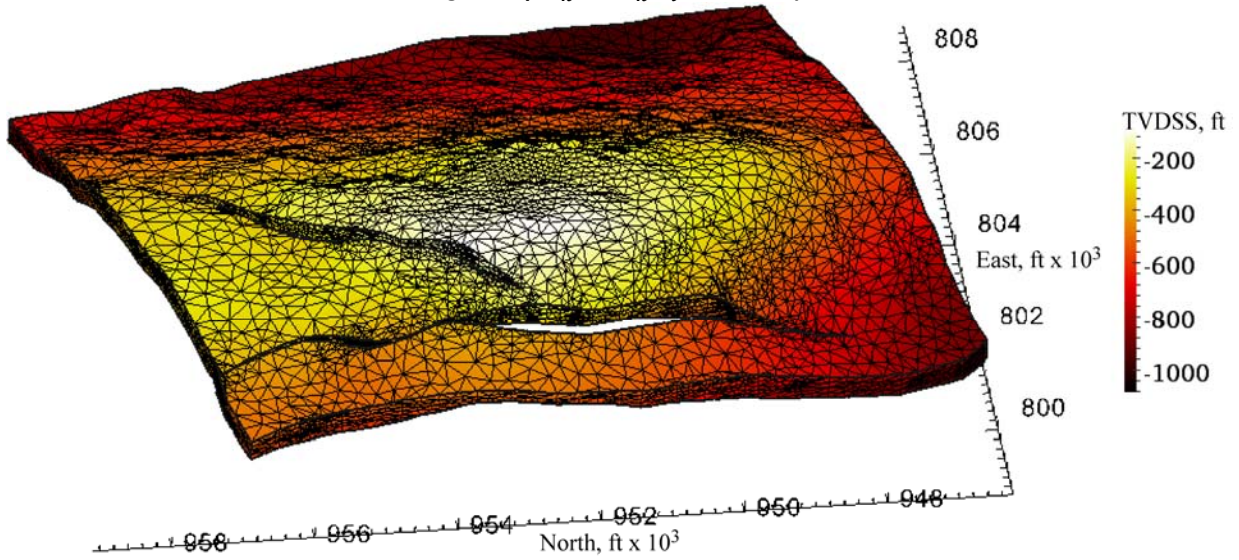


Figure 7: Isometric view of tetrahedral grid design.

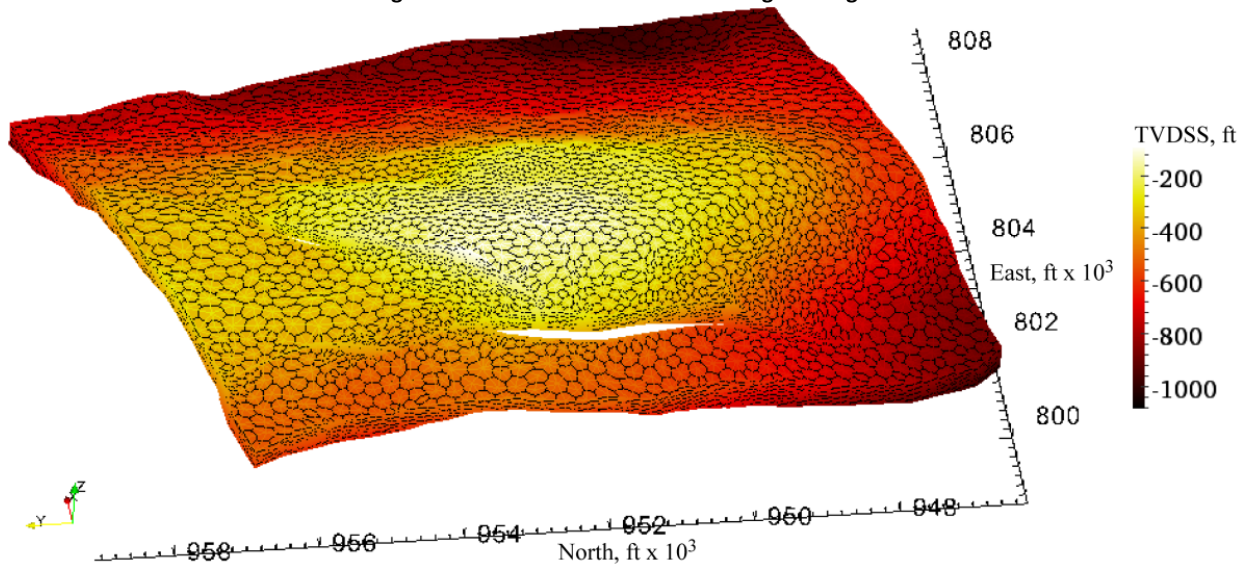


Figure 8: Isometric view of dual polygonal grid.

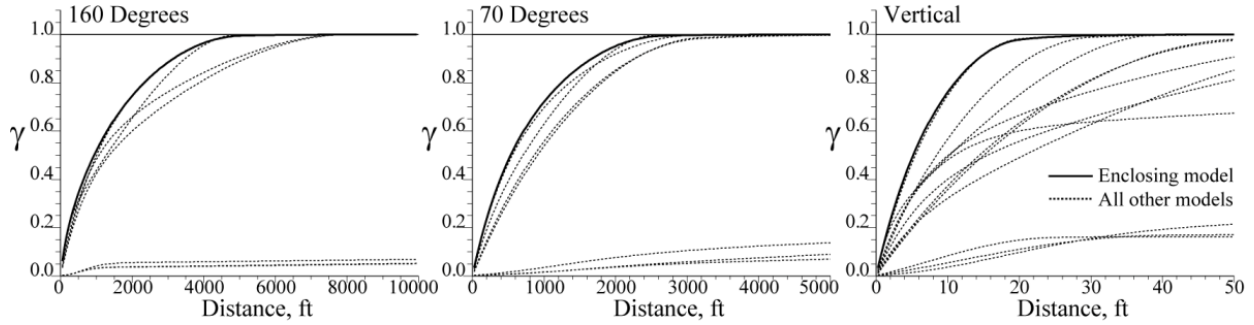


Figure 9: Enclosing variogram model for refinement error.

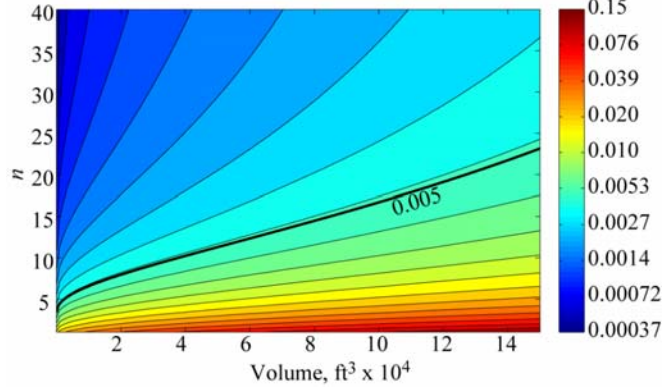


Figure 10: Tetrahedral grid refinement error surface.

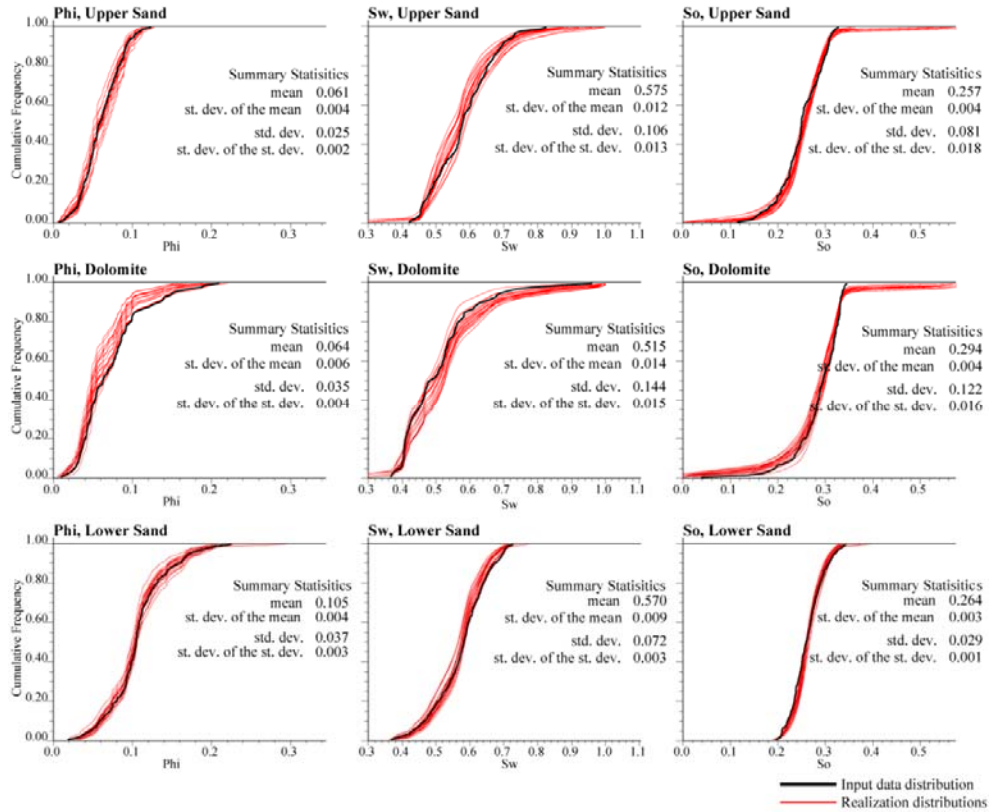


Figure 11: Reproduction of distributions from pgsim realizations.

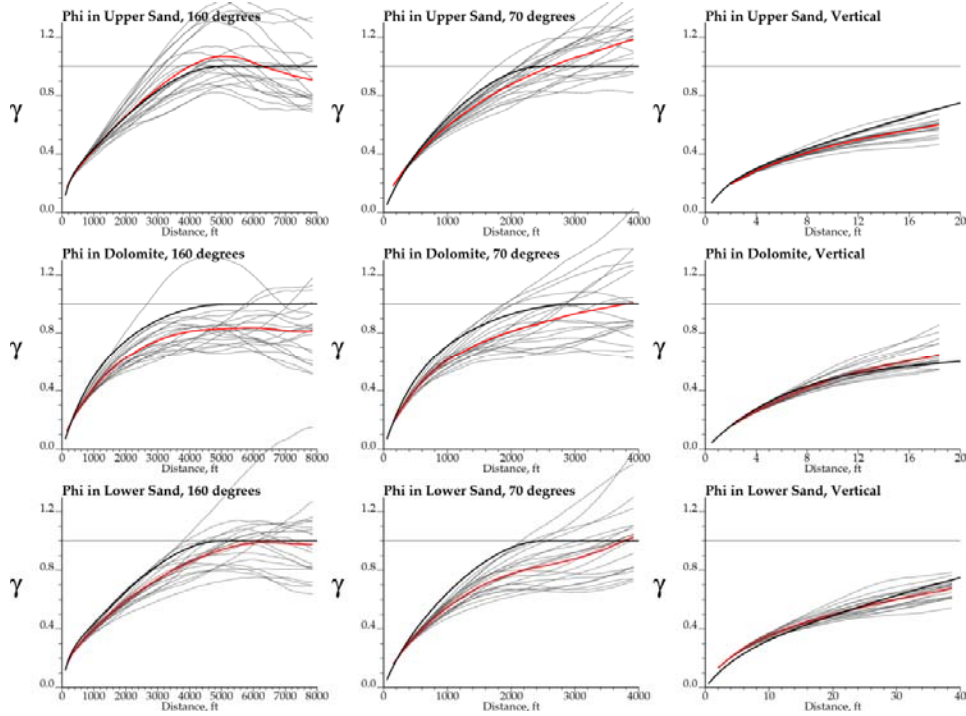


Figure 12: Phi variogram reproduction.

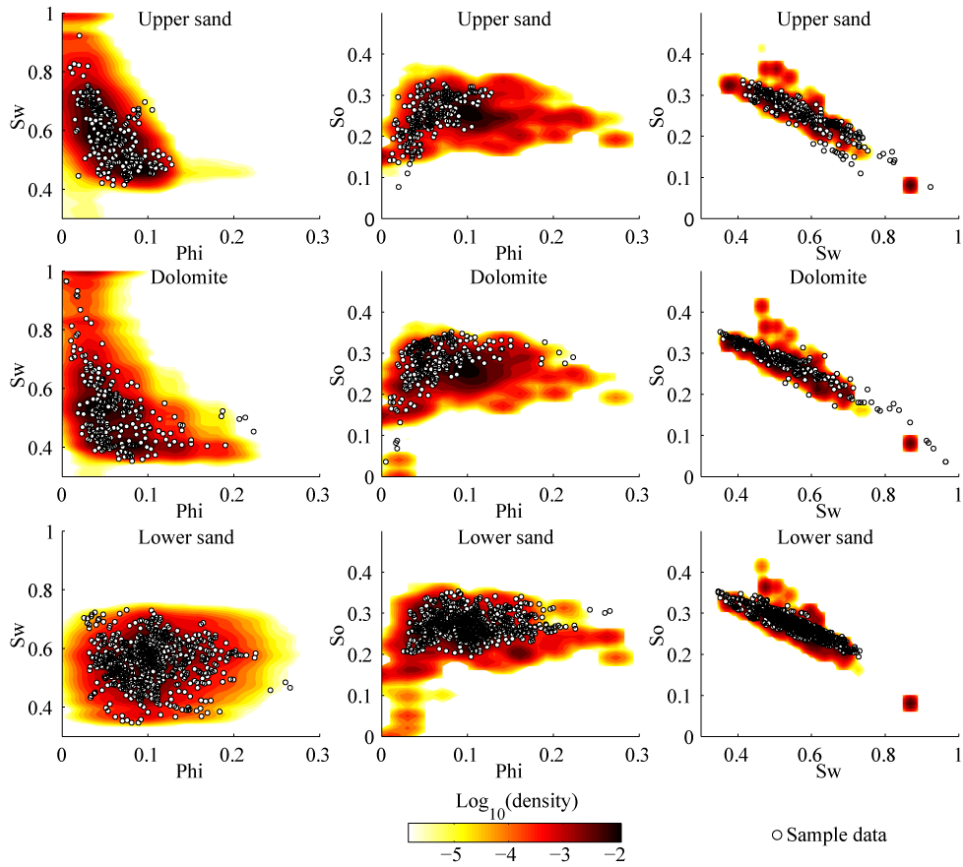


Figure 13: Reproduction of bivariate relationships.

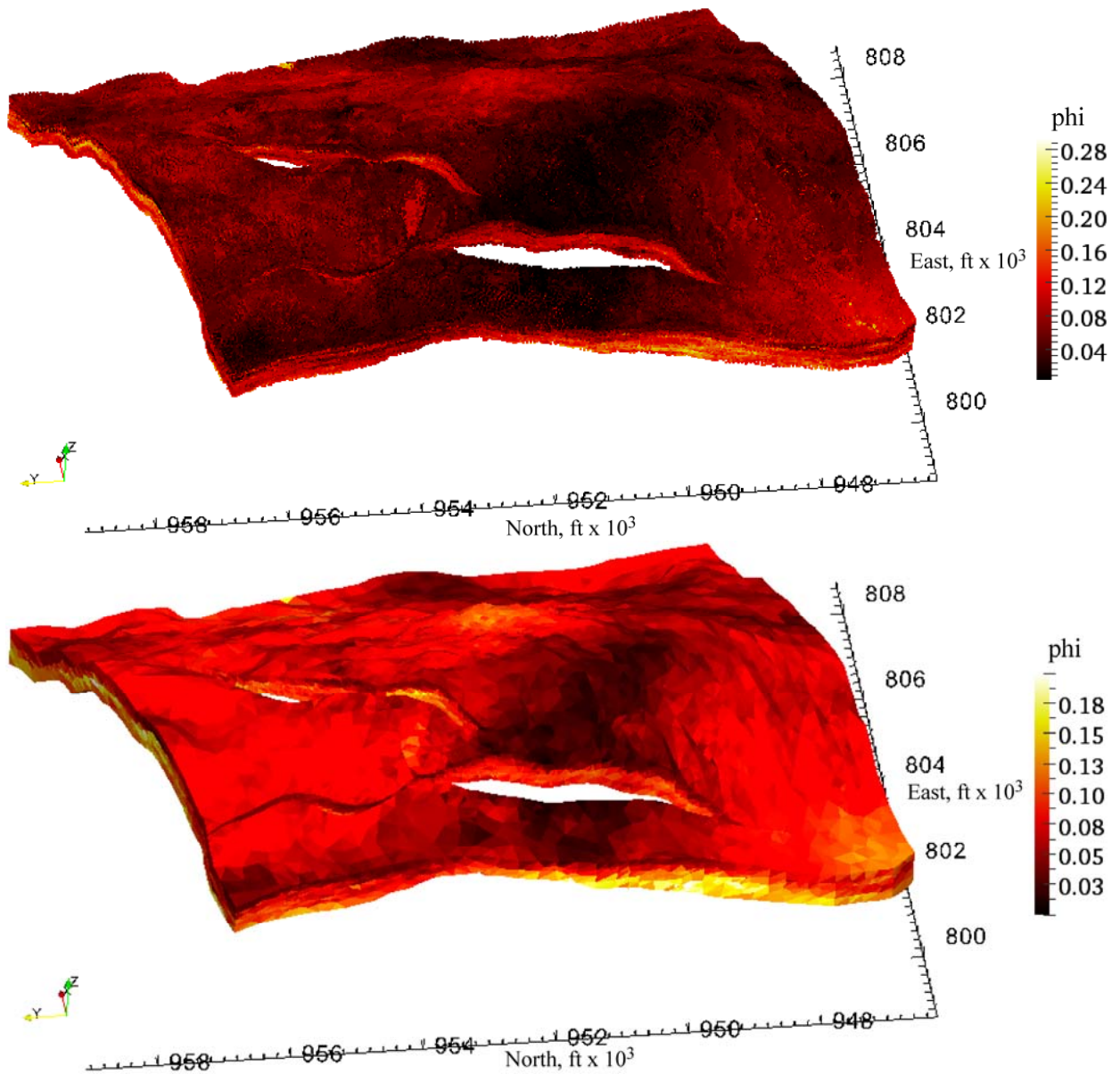


Figure 14: Point scale realization of porosity at fine grid barycenters (top) and upscaled result. A vertical exaggeration of five is used.